This manuscript has been sent for publication to Remote Sensing of Environment. Please note that, despite having undergone peer-review, the manuscript has yet to be formally accepted for publication. Subsequent version of this manuscript may have slightly different content. If accepted, the final version of this manuscript will be available via the 'Peer-reviewed publication DOI'. Please feel free to contact any of the authors. ; we welcome feedback.

Impact of altimeter-buoy data pairing methods on the validation of Sentinel-3A coastal significant wave heights

Guillaume Dodet[a], Grégoire Mureau[b], Mickaël Accensi[a], Jean-François Piollé[a]

[a] *Univ Brest, Ifremer, CNRS, IRD, LOPS, Plouzané, F-29280, France*
[b] *Ifremer, IRSI, ISI Service Ingénierie des Systèmes d'Information, Plouzané, F-29280, France*

Abstract

Sea state information is critical for a broad range of human activities (e.g. shipping, marine energy, marine engineering) most of them being concentrated along the coastal zone. Satellite altimeter records of significant wave heights (SWH) represent the largest source of sea state observations available to date. However, the quality of altimeter observations is reduced in the coastal zone due to surface heterogeneity within the radar signal footprint. Major difficulties to assess the performance of coastal altimetry in the coastal zone are the reduced number of valid altimeter records and the increased sea state variability, which have recently fostered the development of new methods to pair and compare nearby altimeter and buoy data. In this study, we use a high-resolution numerical wave model implemented over the European coastal waters in order to characterize the spatial variability of sea states in the proximity of coastal in situ buoys, we explore different model-based data pairing methods to account for coastal sea state variability and we assess their impact on the validation of Sentinel-3A 20Hz SWH measurements. Three Sentinel-3A processing modes are considered: the pseudo low rate mode processing, the SAR processing and the Low Resolution with Range Migration Correction (LR-RMC) processing. Our results indicate major impacts of data pairing methods on the S3A coastal validation and reveals the contribution of more frequent low SWH conditions, poorly resolved by radar altimeters, in the coastal zone as an additional source of errors in coastal altimetry.

Keywords: Coastal altimetry, Data pairing methods, Sea state variability, Sentinel-3A measurements

1. Introduction

Collecting long-term, frequent and accurate coastal sea state information is critical for a broad range of human activities, such as commercial shipping, harbour operations, marine and coastal engineering, or marine energy resource assessment (Ardhuin et al., 2019). A particularly important demand for coastal sea state data concerns extreme wave statistics, since long return period events are currently significantly underestimated in global wave reanalysis (Fanti et al., 2023) while they may have dramatic impacts on the nearshore environments (Casa-Prat et al., 2024). Moreover, accurate coastal sea state information is required for satellite altimetry applications. Indeed, ocean waves are known to modify the scattering properties of the sea surface, with higher reflectivity in the wave troughs than in the wave crests, resulting in an underestimation of the mean sea level of the order of a few percents of the significant wave height (SWH) (Yaplee et al., 1971; Jackson, 1979). This so-called sea state bias still represents one of the major source of errors in satellite altimeter range corrections in the coastal zone (Vignudelli et al., 2019).

Satellite altimeter records of SWH represent the most abundant archive of sea state observations available to date. However, the quality of altimeter acquisitions is degraded in the coastal zone due to land contamination and sea surface heterogeneities (e.g. natural and oil surface slicks, stretches of calm water in sheltered areas, bottom-induced wave steepening and breaking) within the radar signal footprint (Vignudelli et al., 2019). Over the last decades, increasing efforts have been devoted to enhance the exploitation of altimeter observations closer to the coast using new sensor technologies (e.g. Ka-band and synthetic aperture radar altimeters), improved waveform retracking algorithms (e.g. Passaro et al., 2018; Tourain et al., 2021; Schlembach et al., 2022) , optimized geophysical corrections in the coastal zone (e.g. Fernandes et al., 2015) or dedicated post processing techniques (e.g. Birol et al., 2017) . Among the recent innovations, synthetic aperture radar (SAR) altimetry (also known as Delay-Doppler altimetry) appears particularly efficient for monitoring the coastal zone, thanks to a finer along-track-resolution and a lower noise level (Raney, 1998). In this study, we investigate the performance of the SAR Radar Altimeter (SRAL) instrument on-board the Copernicus Sentinel-3A mission, to retrieve SWHs in the coastal zone. In particular, different processing methods permitted by this instrument, described in the next Section, will be compared.

A number of studies have explored the performance of altimeter missions for measuring wave heights in the coastal zone based on comparisons with in situ measurements (e.g. Hithin et al., 2015; Nencioli and Quartly, 2019; Jiang et al., 2022) and high resolution numerical wave models (Schlembach et al., 2020; Alday et al., 2022). Two major difficulties have been identified for the interpretation of coastal altimeter validation results. On one hand, the number of invalid altimeter data drastically increases close to the coast so that improved error metrics (e.g. bias, root-mean-square error) are often obtained at the expense of a reduced sample size resulting from a more restrictive data editing (Schlembach et al., 2020). On the other hand, the representativeness error due to the spatial and temporal separation distances between pairs of altimeter and in situ measurements strongly increases in the coastal zone and customary collocation method based on fixed thresholds (usually 50km and 30min) are no longer adequate. To overcome these limitations, several authors developed data pairing methods for the coastal zone based on numerical wave model results. Nencioli and Quartly (2019) used wave model hindcast results over the south west coast of England in order to define high correlation areas between buoy and surrounding nodes. The selection of altimeter data to be compared with the buoy data is then based on these high correlation areas, so that spatial representativeness error is reduced. Jiang et al. (2022) revisited this experiment and proposed a dynamic correction to the buoy measurements based on wave model outputs in order to account for SWH variability without reducing the number of altimeter-buoy matchups.

In this study we use a high-resolution numerical wave model implemented over the European coastal waters in order to characterize the spatial variability of sea states in the proximity of 70 coastal in situ buoys. Buoy representativeness areas are defined from the computation of systematic and random errors between the time series simulated at the station and those of neighboring grid points. These areas are then used to compute buoy – altimeter matchup statistics and estimate altimeter errors with respect to the buoy data. Additional methods considered in this study are based on the dynamic comparison between model results at the buoy location and at the altimeter ground measurement, to ensure that (modelled) spatial variability is low before comparing altimeter and in situ data. The impact of these different data pairing methods on the coastal performance of Sentinel-3A (S3A) SWH measurements is then investigated. S3A SWH measurements obtained with PLRM, SAR and LR-RMC processing methods are considered. A particular attention is given to the impact of the data pairing methods on the geographical sampling and SWH distribution in coastal altimeter records. The S3A, buoy and model dataset are presented in the next section (Section 2), followed by a description of the methods implemented to compute the buoy representativeness areas, the different data pairing methods, and the S3A performance metrics in Section 3. In Section 4, we present first the buoy representativeness areas along the coast of Europe, we then analyse the impact of the data pairing methods on the overall S3A performance, and we investigate more particularly the spatial and SWH distribution of sampled altimeter data. Finally, the coastal performance of S3A SWH measurements are presented and discussed to the lights of the improved comprehension of the impact of data pairing methods. Section 5 provides a summary of the results and presents some perspectives of application.

2. Datasets

2.1. Sentinel-3A

The Copernicus Sentinel-3A (S3A hereafter) mission, launched in February 2016, is a low Earth polar orbiting satellite operating at an average altitude of 815 km above the Earth surface with a repeat cycle of 27 days. It carries onboard a SAR Radar Altimeter (SRAL), which provides high-resolution SWH measurements. SAR altimetry was first developed for the European Space Agency (ESA) mission Cryosat for its measurements over ice (and later extended to small sample regions of the ocean), but S3A is the first altimeter mission to operate in SAR mode globally over all surfaces. SAR altimeters present a narrow ($\sim 300m$) footprint in the along-track direction , which present a major advantage in comparison to conventional low rate mode (LRM) altimetry for which the diameter of the altimeter footprint can exceeds 10km during rough sea state conditions (Chelton et al., 1989)making each consecutive 20Hz measurements (approximately 300m apart) dependent to each other. The SAR narrow-band footprint results from the coherent processing of radar pulses transmitted at very high rate (ten times as high as for LRM) to localize radar echoes and form multi-looked waveforms (Raney, 1998). Despite its clear advantages in terms of resolution and noise level (Boy et al., 2017), SAR processing has also proven to be particularly sensitive to the presence of swells for retrieving accurate wave height information (Moreau et al., 2018). Moreover, the 20Hz sampling was found to inadequately sample high frequency ocean wave signals, inducing errors over the entire wavenumber spectrum through spectral aliasing (Rieu et al., 2021; Ehlers et al., 2023). To overcome this issue, Moreau et al. (2021) implemented the Low Resolution with Range Migration Correction (LR-RMC hereafter) method, which uses an alternative averaging (stacking) operation so that all the Doppler beams produced in a radar cycle (4 bursts of 64 beams for the S3 open-burst mode) are incoherently combined to form a multi-beam echo. Contrarily to the narrow-band SAR technique, the LR-RMC processing enlarges the effective footprint to average out the effects of surface waves that are known to impact SARprocessing performances. As a consequence, the measurements between successive 20Hz records are not independent anymore. On the other hand, the number of averaged beams is as high as in current SAR processing, thus providing a noise reduction at least equally good.

The S3A measurements considered in this study are along-track SWH records at 20Hz posting rate (corresponding to approximately 300m spacing between two records) over the period January 2018 - December 2020. The SWH measurements are estimated from three different processing methods, namely the Pseudo Low Resolution (PLRM), SAR and LR-RMC methods. The PLRM and SAR data are both from the EUMETSAT SRAL/MWR L2 Marine products (https://www.eumetsat.int/sentinel-3), while the LR-RMC data are from the ESA Sea State Climate Change Initiative project (https://climate.esa.int/en/projects/sea-state/). For each dataset, data editing was performed based on the available surface type and quality flag information.

2.2. Wave buoys

The CMEMS In Situ Thematic Assembly Center (CMEMS INSTAC) is a component of the CMEMS and its role is to ensure consistent and reliable access to a range of in situ data for service production and validation. For this purpose, CMEMS INSTAC collect multi-source/multiplatform data, and perform consistent quality control before distributing the data in a common format to the CMEMS Marine Forecasting Centres (MFC). The data can be found at http://www.marineinsitu.eu/. In this study, we considered all wave buoys moored in locations within 20km from a Sentinel-3A track and at a 1-km minimum distance to the coast. 70 buoys were identified, with distance to the coast comprised between 2 and 250 km. Almost 70% of these buoys are located within 50km from the coast while the remaining 30% provide a means of comparisons between offshore and coastal environments. The locations of these buoys are shown on Figure 1.

2.3. High-resolution numerical wave model

The wave model hindcast used in this study is being developed at IFREMER in the context of the ResourceCODE project (OCEAN ERA-Net cofound) with the aim to provide accurate long-term sea state information for the exploitation of Marine Renewable Energy (https://resourcecode.ifremer.fr/). It is a regional implementation of the WAVEWATCH III (hereafter WW3) spectral wave model on a high-resolution unstructured mesh extending from the south of Spain to the Faroe Islands, and from the western Irish continental shelf to the Baltic Sea (12°W to 13.5°E, 36°N to 63°N). The extension of the model grid is presented on Figure 1 with an example of simulated SWH field during Ulla storm on February, 14 2014. The hindcast covers a 28-year period, from 1993 to 2020 , and gridded outputs are stored every hour. The bathymetry combines data from the EMODnet dataset (EMODnet 2016) and the HOMONIM dataset provided by the French Naval Hydrographic

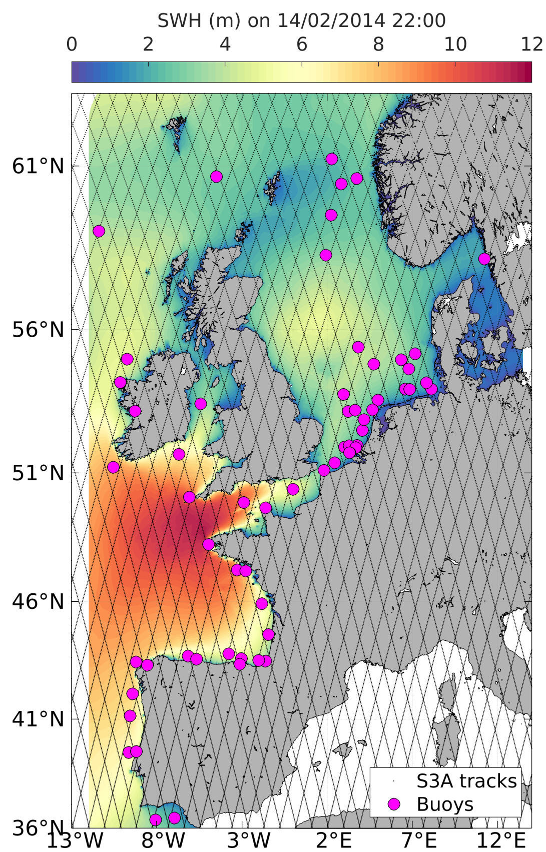

Figure 1: Location of the 70 wave buoys (magenta circles) moored within 20 km of Sentinel-3A ground tracks (dashed black lines) selected for this study. The background colorscale shows the SWH field from the high-resolution wave model during Ulla storm (February 14 2014).

and Oceanographic Service (Shom) with a 0.001° resolution over the Channel and the Bay of Biscay. The spatial mesh contains 328,000 nodes and the resolution ranges from 10 km offshore to 200 m near the coast. The spectral grid consists of 36 directions and 36 exponentially spaced frequencies, from 0.0339Hz to 0.9526Hz. The physical parameterization corresponds to test T475, as described in Alday et al. (2021), which uses adjusted parameters for the wind-wave generation and swell damping terms. The model is forced along its boundaries with wave spectra generated by a global WW3 wave model hindcast forced with ERA-5 hourly wind fields (Hersbach et al., 2020) and CMEMS-Globcurrent surface current fields (Global Ocean Multi Observation Product, MULTIOBS_GLO_PHY_REP_015_004). The regional model is forced by ERA-5 wind fields (with a bias correction for wind speeds larger than 21m/s), and with currents and water levels reconstructed from the MARS2D and FES2014 tidal harmonics database. Detailed information on the ResourceCODE model implementation and validation can be found in Accensi et al. (2021) and Alday et al. (2022). Moreover, implementation and validation of the global wave hindcast are described in Alday et al. (2021).

3. Methods

3.1. Buoy representativeness area

In order to characterize the spatial variability of the SWH in the vicinity of the buoy, and to quantify the spatial representativeness of the buoy SWH measurements, we implemented a methodology based on the results of the high resolution numerical wave hindcast described in Section 2.3, and inspired from the work of Nencioli and Quartly (2019). In this method, the time-series of simulated SWH at the buoy location is compared to the time-series of simulated SWH at every surrounding nodes located within a radius of 200km. The normalized bias (Nbias, Eq.1) and the scatter index (SI, Eq.2) are computed between the buoy and its neighbouring nodes, to characterize both systematic and random variabilities, respectively. The NBias and SI values are then interpolated over a 200 x 200 km regular grid with 200m resolution in order to enhance the sampling in offshore regions, where the unstructured grid has a coarser resolution. The area presenting Nbias and SI values lower than 5% is then identified as the buoy representativeness area and a polygon is fitted to encompass this area as closely as possible. The different steps of the methods are illustrated on Figure 2 for buoy 6200080, which is located nearby La Rochelle, on the west coast of France. Note that this method can be applied to other sea state parameters, such as the wave period and direction as in Mureau et al. (2022), and other geophysical variables for which satellite-in situ collocation is required, for instance to investigate coastal sea level variability nearby tide gauges.

Given that sea states present significant seasonal, inter-annual, and decadal variability, it is expected that the buoy representativeness areas depends on the time period over which they are computed. In this study, we have considered stationary buoy representativeness areas and we have used a 10-year time window from the model hindcast to compute these aeras. The polygon vertices of the representativeness areas for the 70 European buoys considered in this study are provided as Supplementary Material (SM1), so that similar coastal validation activities can be performed.

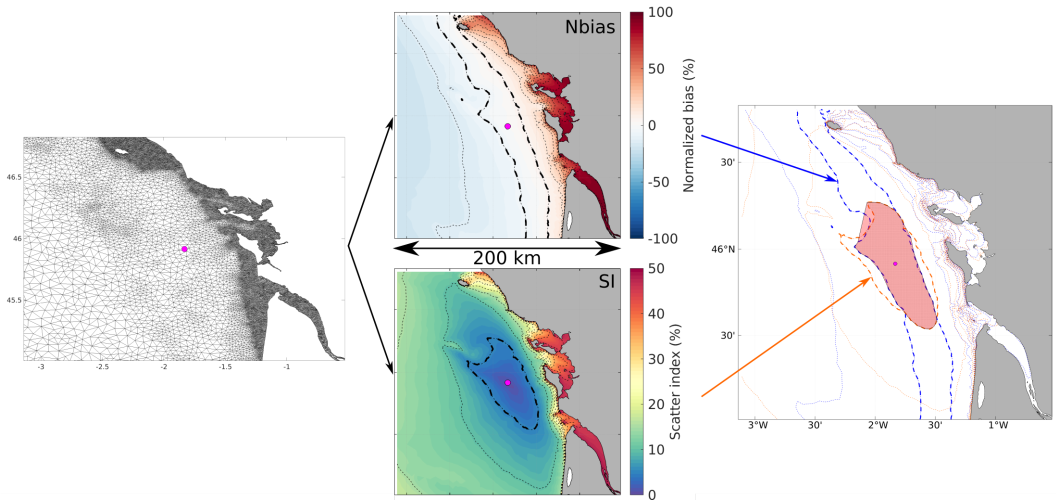

Figure 2: Processing of the buoy representativeness area for buoy 6200080 (nearby La Rochelle, France). Step1 (left panel): Differences between modelled SWH at buoy location and surrounding nodes are computed over the hindcast duration. Step2 (middle panel): Maps of normalized bias and scatter index are interpolated over 200kmx200km grid (tick black dashed lines indicate the 5% isocontour). Step3 (right panel): The intersection (dotted area) between areas with |Nbias| <5% (thick blue dashed line) and SI<5% (thick orange dashed line) is used to fit a convex polygon casting the buoy representativeness area (red shaded area).

3.2. Data pairing methods

Data pairing methods (also known as collocation or matchup detection methods) are required to associate and compare values acquired by distinct measurement systems (model or sensor) at nearby location and time (e.g. satellite and in situ observations). Four data pairing methods are considered in this study. These methods are based on spatial criteria only since wave buoy measurements usually provide continuous hourly records, giving a maximum separation time between satellite and buoy records of 30min, which is sufficiently small to consider the sea state to be stationary. The four methods are:

1. The *static* method: it uses a fixed separation distance (radius) from the buoy location to sample all altimeter records within this distance. This method is used in most altimeter CAL/VAL studies based on in situ measurements. The selected threshold is usually 100km, but it can be relaxed to 300km in order to increase the number of available data pairs. Conversely, on the coastal zone this distance is often reduced but barely below 20km to keep a sufficient number of available data pairs. In this study we consider four separation distances : 100, 50, 20, and 5km.
2. The *polygon-based* method: it uses the polygon vertices derived from the buoy representativeness area analysis (see Section 3.1) to sample only the altimeter records within the area (polygon) of low sea state variability. The maximum separation distance is 100km. This method is adapted from the definition of areas of correlation elaborated by Nencioli and Quartly (2019).

3. The *dynamic collocation* method: it uses model results dynamically (i.e. model results are analysed at the time of altimeter measurements) to sample only the altimeter records for which modelled SWH difference between the buoy and the altimeter locations is below 5%, following Janssen et al. (2007). The maximum separation distance is 100km.
4. The *dynamic correction* method: it uses the model results dynamically in order to correct the buoy measurement from the modelled SWH gradient between the buoy and the altimeter record location. In its original form, proposed by Jiang (2020), this method gives the possibility to use several buoys , with a weighting scheme based on the inverse squared distance between each buoy and the altimeter records, to characterize more precisely the sea state conditions at the altimeter record location. Note that this method does not constrain the altimeter record sampling and can actually be used in combination with any of the method presented above. In this study we have considered the method in its simplest form (only one buoy is used for a given location, see Equation 3 in Jiang, 2020) and a fixed maximum separation distance of 50km.

Examples of sampling obtained with the static, polygon and dynamic collocation methods for buoy 6200192, nearby Nazaré in Portugal, are shown on Figure 3. Selected and rejected samples are shown as blue and black dots, respectively. For the static (left panel) and polygon (middle panel) methods, all altimeter records located within the sampling area (red shaded area) are selected, while for the dynamic collocation method (right panel), the sampling area varies at each satellite pass depending on the modelled SWH gradient. However, we see that with this latter method, altimeter records as far as 100km from the buoy can be selected.

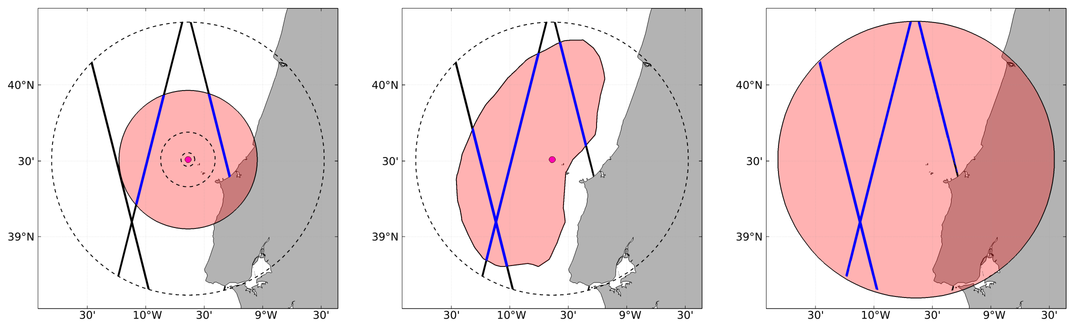

Figure 3: Examples of sampling regions (red shaded area) and altimeter records (blue dots) paired with buoy 6200192 (magenta circle) for the different data pairing methods. (left) the *static* method considers only measurements within a fixed separation distance (here 50km) from the buoy; four distances are considered: 100, 50, 20 and 5km (black circles); b) the *polygon-based* method considers only measurements occurring within the buoy representativeness area estimated from model hindcast; c) the *dynamic collocation* method considers only measurements within 100km from the buoy for which modelled SWH difference between the buoy and the altimeter record is lower than 5%. Black dots represent altimeter records that are not selected for comparisons.

3.3. Evaluation of S3A performance

S3A performance in the coastal zone was evaluated through statistical comparisons against buoy SWH records. The selected metrics for these comparisons are the normalized bias (Nbias), the scatter index (SI), and the correlation coefficient(R), computed as follows:

$$Nbias = \frac{\sum(A_i - B_i)}{\sum B_i} \tag{1}$$

$$SI = \sqrt{\frac{\sum[(A_i - \bar{A}_i) - (B_i - \bar{B}_i)]^2}{\sum B_i^2}} \tag{2}$$

$$R = \frac{\sum(A_i - \bar{A}_i)(B_i - \bar{B}_i)}{\sum(A_i - \bar{A}_i)^2 \sum(B_i - \bar{B}_i)^2} \quad (3)$$

For the S3A-buoy data comparisons, the metrics were computed using all the data pairs obtained with each of the four data pairing methods presented previously. As opposed to previous altimeter validation work, in which the altimeter records collocated with buoy data are averaged using along-track neighbour data (which is generally referred to as "super-observations") to reduce high-frequency noise (e.g. Abdalla et al., 2011), we consider here raw altimeter records, without any averaging, in order to estimate the uncertainty associated to the noisy individual 20Hz record. Similarly, no smoothing was applied to the buoy data and only the buoy SWH recorded at the closest time to the altimeter approach was used for comparison.

4. Results and discussion

4.1. Wave buoy representativeness areas

SWH representativeness areas were computed for the 70 buoys selected for this study, from the analysis of the high resolution wave hindcast (see Section 2.3). These areas, shown on Figure 4, exhibit strong heterogeneities in size and shape. In particular, offshore buoys (i.e. with distance to coast larger than 50km, as defined in this study) are characterized by low and isotropic SWH variability resulting in large and near-circular representativeness areas, with mean and maximum surface areas of 4,000 and10,000km^2, respectively (i.e. with an equivalent radius of 35 and56km , respectively), while nearshore buoys present very local error gradients resulting in reduced representativeness areas with surface areas as low as 7 km^2 (i.e. with an equivalent radius of 1.5km). Buoys at intermediate distance from the coast present significant cross-shore error gradients (not shown here) resulting in anisotropic representativeness areas stretched in the along-shore direction. Note that many buoys moored in the North Sea at more than 100km from the coast present smaller representativeness areas than several buoys moored in the Atlantic ocean at less than 50 km from the coast (e.g. along the western Portuguese coast), meaning that the distance to the coast is not the only factor influencing sea state variability. Although it is not the goal of this study to investigate which environmental factors controls the coastal sea state variability depicted by the buoy representativness area, we hypothesize that coastline geometry, and bathymetry, current and wind gradients are the main factors explaining coastal sea state variability, as investigated by many authors (e.g. Abdalla and Cavaleri, 2002; Ardhuin et al., 2012; Dodet et al., 2019). Several conclusions can be drawn from this preliminary analysis. First, since the most exposed buoys present quasi-circular representativeness areas of roughly 50-km radius, we can say that the (static) 50-km maximum separation distance often used to collocate altimeter and offshore buoy measurements (e.g. Zieger et al., 2009; Queffeulou, 2004) may explain at least 5% of systematic and random spatial representativeness errors in standard CAL/VAL studies using offshore buoys only. Then, we see that using the distance to the coast to select buoy data for comparison with (distant) satellite measurements is not sufficient to discriminate buoys with low and high spatial variability, and other parameters should also be considered (e.g. current and wind gradients, degree of exposure to oceanic swell and wind sea). Finally, the very confined representativeness areas of some near coastal buoys, such as buoy 6200059 (Cherbourg, France), clearly hinders their use for satellite CAL/VAL activities.

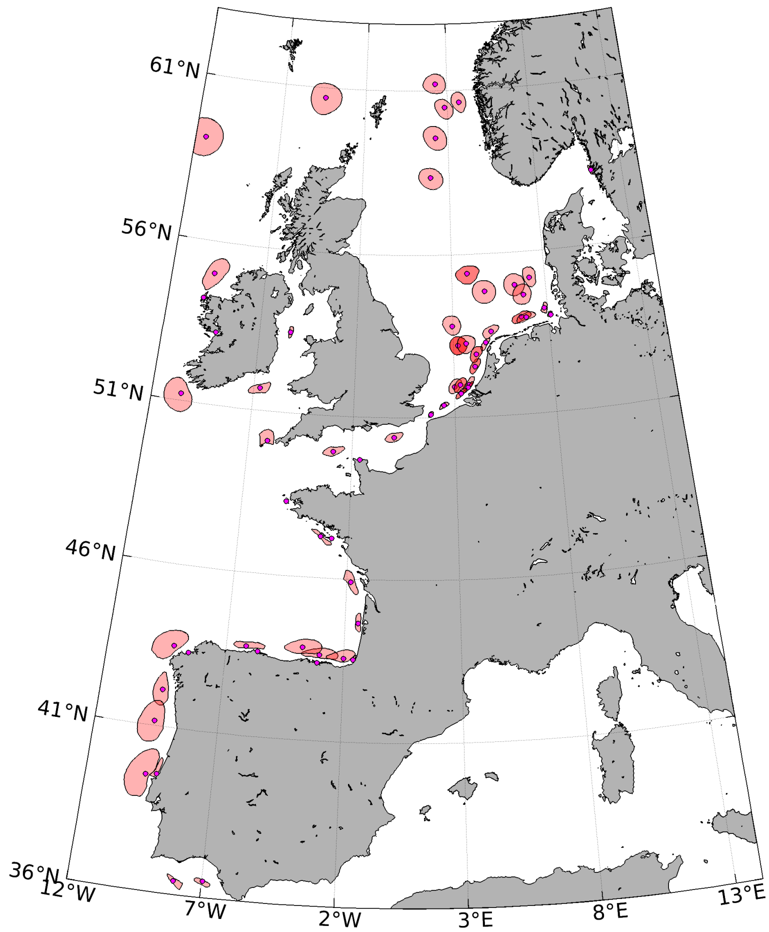

Figure 4: Map showing the buoy locations (magenta circles) and buoy representativeness area polygons (light red areas) computed for 70 European buoys selected for this study.

4.2. Sensitivity of S3 coastal validation to data pairing methods

In Section 3.2 (Figure 3), we have shown that the choice of the data pairing method has a strong influence on the geographic sampling of altimeter records to be compared with the buoy measurements. This choice is therefore expected to impact the error metrics computed from these comparisons. In order to investigate the sensitivity of altimeter validation results to the data pairing methods, we compared Sentinel-3A SAR and buoy data using data pairs given by the static, polygon, dynamic collocation and dynamic correction methods. For each method we computed the relative (with respect to the 100km-static method) number of data pairs ($Nval$), the normalized bias ($Nbias$), the scatter index (SI), and the correlation coefficient(R). Figure 5 compares the different metrics obtained with the four data pairing method, the first four bars corresponding to the four separation distances used with the static method (100km, 50km, 20km and 5km).

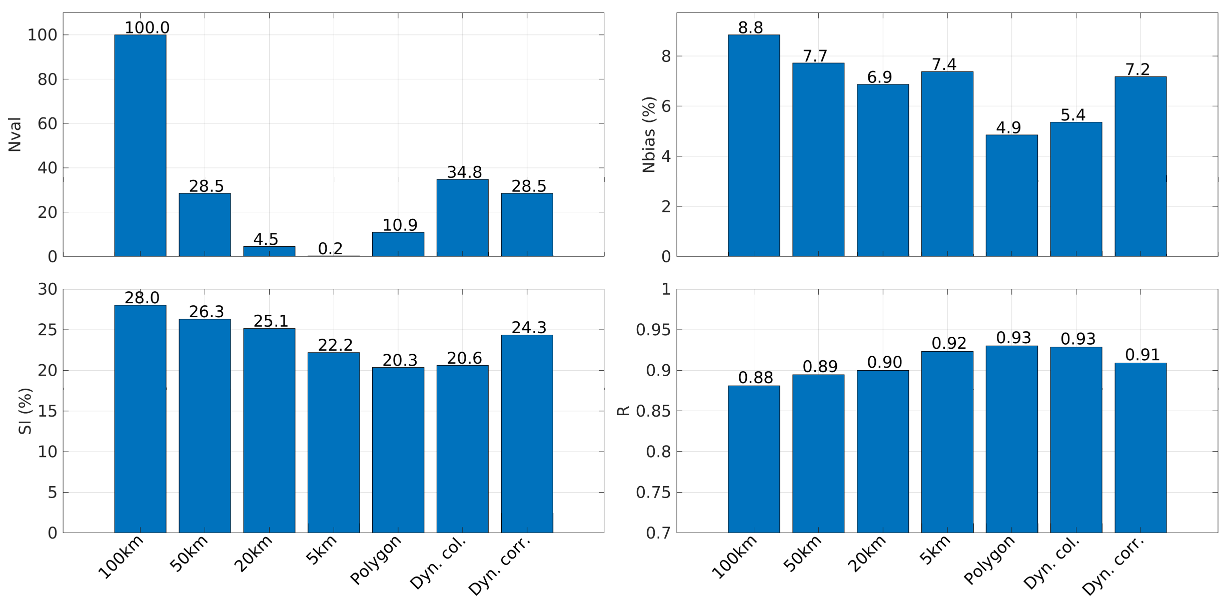

Figure 5: Relative number of data pairs ($Nval$), normalized bias ($Nbias$), scatter index (SI), and correlation coefficient(R) obtained from the comparisons between Sentinel 3A SAR and buoy SWH data for the different data pairing methods.

Looking at the relative number of data pairs ($Nval$) obtained with the static method and considering the 100, 50, 20 and 5-km maximum separation distances, we note a rapid decrease of available matchups when the maximum separation distance is reduced, matching the expected inverse-square law of the sampling surface area.Indeed, if we consider that the number of altimeter samples is proportional to the surface area of the considered region, it is therefore inversely proportional to the square of the maximum separation distance. As a result, using a fixed separation distance lower or equal than 20km reduces the number of samples by less than 5% with respect to the number of samples obtained with a 100-km separation distance. Conversely, the three model-based methods (i.e. the polygon-based, dynamic collocation and dynamic correction methods) preserve between 10 to 35% of data . In terms of normalized bias, we see that $Nbias$ is systematically higher for the four static methods and the dynamic correction method (6.9-8.8%) than for the polygon and dynamic collocation methods (4.9-5.4%). Same conclusions can be drawn for SI and R, for which the static and dynamic correction methods shows poorer performance (22.2-28.0% for SI and 0.88-0.92 for R) than the polygon and dynamic collocation methods (20.3-20.6% for SI and 0.93 for R). Overall, the dynamic collocation method gives the best score while preserving a significant amount of data (34.8%). The dynamic correction method, which shares the same sampling than the 50-km static method presents slightly better performance than this latter, thanks to the model-based correction. Similar results were obtained when the same analysis was applied to PLRM and LR-RMC data (not shown here). However, we may question whether such conclusions can be drawn for each buoy separately or only for the aggregated dataset. To answer this point, we estimated for each buoy which data pairing method provides the best score for the four considered parameters (Figure 6 and Table 1). For this analysis, we only considered the 50km separation distance for the static method, as it provides the best trade-off between the number of samples and the error metrics. First, we see that the maximum number of samples are either ob-

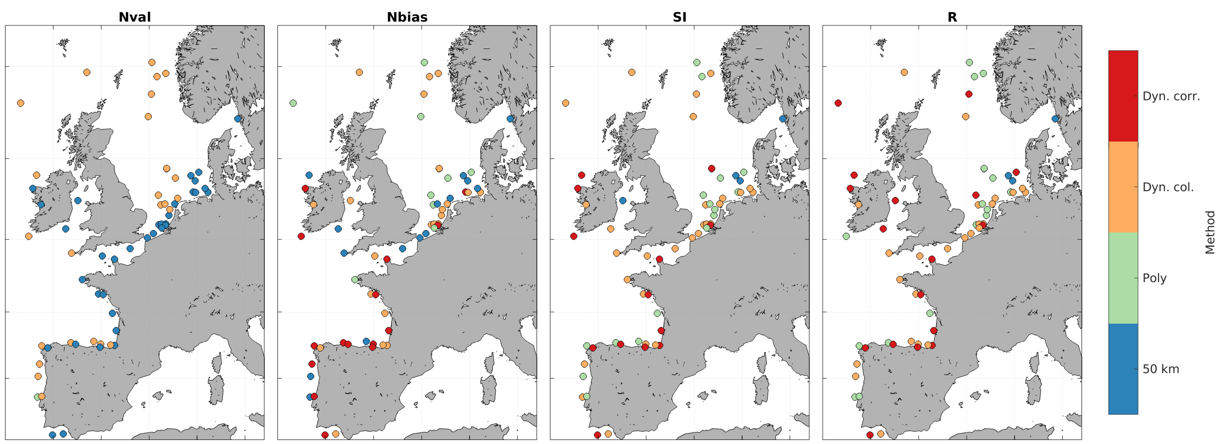

Figure 6: Spatial distribution of the data pairing methods providing the best score at each buoy location for the following metrics: relative number of data pairs ($Nval$), normalized bias ($Nbias$), scatter index (SI), and correlation coefficient(R) obtained from the comparisons between Sentinel 3A SAR and buoy SWH data.

tained with the 50km-static or the dynamic collocation methods (first panel). Note that the dynamic correction method uses the same sampling as the 50km-static method and therefore cannot be differentiated for this parameter (hence blue circles can be swapped with red circles). In terms of spatial distribution, we see that the 50km-static method provides the largest number of samples mostly for buoys located near the coast, while the dynamic collocation methods provides the largest number of samples for the offshore buoys. This can be explained by the fact that - as opposed to the 50-km static method - the dynamic collocation method considers altimeter records within 50-100km from the buoy for which the modelled SWH difference with the buoy location is small. In offshore conditions, a significant number of altimeter records located between 50-100km from the buoy satisfy this condition, as opposed to nearshore conditions where SWH variability is much stronger. The number of samples obtained with the polygon-based method is systematically lower due to site-dependent representativeness areas, which hardly cover an equivalent 50-km radius disc area for the most exposed buoys, and can be so small near the coast that no satellite record intersect it (see Section 4.1 and Figure 4). In terms of $Nbias$ we find that the dynamic collocation method gives the best score (lowest absolute Nbias) for the largest number of buoys (40%), while the polygon method gives the best score for the lowest number of buoys (16%). For SI and R, the three model-based methods are clearly better than the 50km-static method for most buoys, with the dynamic collocation method showing best scores for 44% and 40% of the buoys, respectively. Similar rankings were obtained when the analysis was applied to the PLRM and LR-RMC datasets (not shown here). This analysis highlights the benefits of using model-based information to compare altimeter with buoy data and indicates that, for the set of buoys considered in this study, the dynamic collocation method outperforms the other methods both in terms of systematic and random errors, while the dynamic correction method preserves the largest number of samples. Nevertheless, our results also indicate that buoy settings should be considered individually to select the most adequate collocation method. Moreover, we recall here that the dynamic correction method can be used in combination with any sampling method, so that its performance could be enhanced by applying the polygon-based or dynamic collocation.

Method	Nval (%)	Nbias (%)	SI (%)	R (%)
50km-static	57*	21	6	4
Polygon	1.5	16	29	29
Dynamic collocation	41.5	40	44	40
Dynamic correction	57*	23	21	27

Table 1: Percentage of buoys showing the best score for the following parameters: $Nval$, $Nbias$, SI, R (see also Figure 6). *Note that the 50km-static and Dynamic correction methods share an equal number of values, hence a similar ranking with these two methods and an overall sum different than 100% .

4.3. Impact of data pairing method on sampling geometry and SWH distribution

Several factors may explain increased altimeter-buoy errors in the coastal zone: first, the sampling pattern of altimeter data collocated with coastal buoys is often skewed offshore (wrt. buoy position) because a higher fraction of altimeter data is invalid near the coast. Given that coastal sea states attenuate towards the coast (e.g. Passaro et al., 2021), there is a dominance of higher-than-average altimeter SWH in the selected samples, as explained by Jiang (2022) ; second, radar altimeter sensors do not have a sufficient range resolution (around 50cm for Ku-band instruments) to resolve low sea states (Smith et al., 2015), which could result in increased error level near the coast where sea states are lower on average. In order to investigate how the different data pairing methods influence the spatial sampling, Figure 7 (left) shows histograms of the relative distance to the coast computed as the difference between the altimeter distance to the coast and the buoy distance to the coast, with altimeter records selected with three different data pairing methods (50-km static, polygon and dynamic collocation). Positive values correspond to altimeter-buoy matchups when the satellite is at a greater distance from the coast than the buoy and negative values correspond to altimeter-buoy matchups when the satellite is at a lower distance from the coast than the buoy. In the former case, the altimeter is likely to measure lower (respectively higher) SWH than the buoy, although the inverse is also possible in certain coastal configurations. For this analysis, only matchups obtained with buoys located within 50km from the coast were used. We

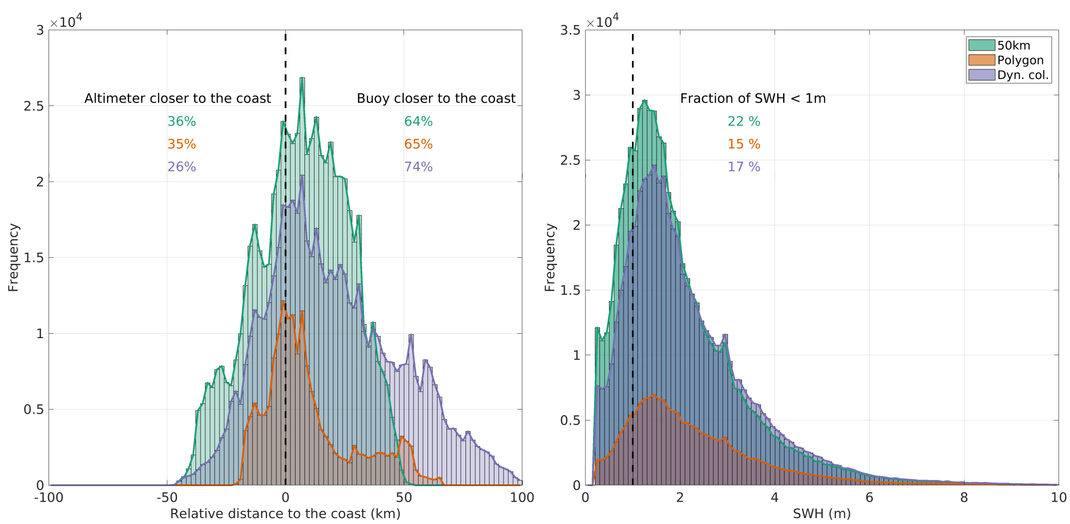

Figure 7: Histograms of the relative distance to the coast computed as the altimeter minus the buoy distance to the coast (left), and SWH (right) for the 50km-static (green), polygon (orange) and dynamic collocation (blue) methods. Only matchups with buoys located within 50km from the coast are considered here.

see that the distributions are all right-skewed, regardless of the data pairing method. The histogram of the 50km static method (green) is bounded at 50km on either side of the buoy location, as expected, with 64% of positive values. The polygon method (orange) samples a lower number of values than the other methods, mostly bounded between -25km and 60km, and 64% of positive values. The histogram of the dynamic collocation method (blue) is the most skewed, bounded between -50km and 100km, and with 74%positive values with the dynamic collocation method showing the highest excess of positive values (74%). Assuming that waves have generally more energy offshore than on the shoreward side of the buoy (see for instance Figure 2 of Mureau et al. 2022), we could expect a larger proportion of large waves with this last method, which could partially explains the larger bias obtained with this method in comparison to the other model-based methods (see Figure 5). On the SWH histograms shown on Figure 8 (right), we see that the choice of the method has a significant impact not only on the total number of samples but also on the sampling distribution, with a higher proportion of low sea state (below 1m) with the static method.

In order to investigate the impact of the significant wave height on the systematic and random errors between altimeter and buoy measurements, the NBias and SI parameters were computed as a function of the buoy SWH (Figure 8, left). Only altimeter records and buoys located at more than 50km from the coast were considered in order to reduce the impact of any coastal effects (e.g. land contamination of the footprint). We see that NBias is almost constant (around 4%) for SWH between 2-6m and rapidly increases for SWH below 1 m, exceeding 100% for the 0-0.5m bin. For SI, the increase is more gradual and become significant for SWH below 2m, exceeding 110% for the 0-0.5m bin. On the right panel of Figure 8, the median and standard deviation of SWH as a function of the distance to the coast, for both buoy and S3A measurements. We see that the proportion of SWH below 2 m increases towards the coast, and represents more than half of the samples between 0-10km. Given this higher proportion of calm sea states in the coastal zone, and the increased errors for low sea states, we can expect stronger (positive) systematic and random errors when altimeter measurements are compared to near coastal buoys, even when model-based collocation method is used. Such increased error is not directly related to coastal interference with the altimeter radar signal and its significant contribution to the uncertainties on coastal altimeter-derived SWH record is still little documented in existing coastal altimetry studies.

4.4. Evaluation of S3A coastal performance

In the previous section, we have shown that the use of any of the three model-based data pairing methods (polygon, dynamic collocation, and dynamic correction) to compare S3A and in situ data significantly reduced the spatial representativeness errors induced by the strong SWH spatial variability in the vicinity of the coastal buoys. Moreover, we have shown that the higher fraction of low sea states towards the coast may explain larger errors near the coast. In this section, we will examine the coastal performance of S3A SWH measurements to the light of these findings, considering three S3A processing techniques: PLRM, SAR and LR-RMC. The dynamic collocation method is used to pair S3A with buoy data as it was shown to provide the best results for the largest number of buoys while preserving a large amount

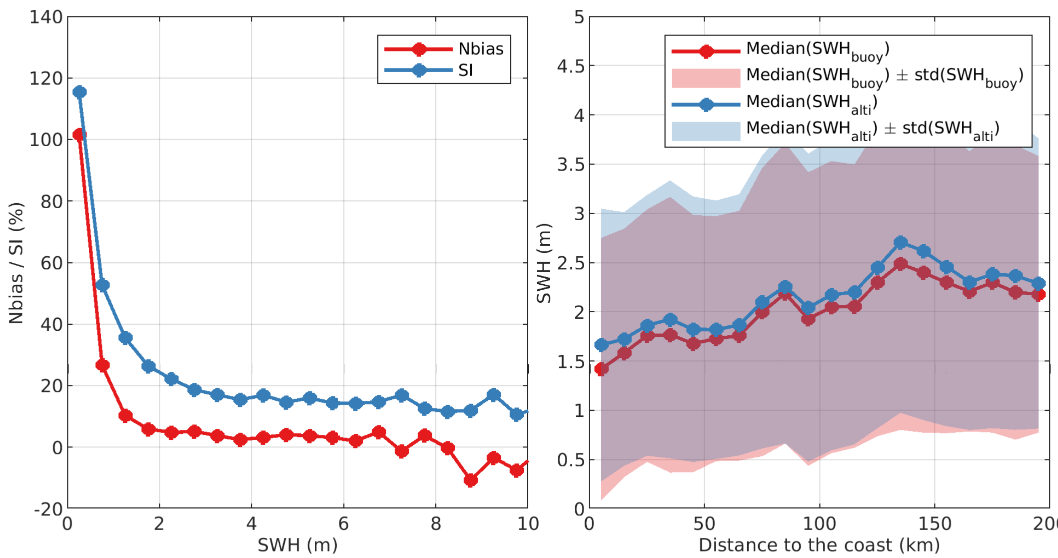

Figure 8: (Left) Nbias (blue) and SI (red) between S3A SAR and buoy data as a function of buoy SWH. Only buoy and alitmeter data located at more than 50km from the coast are used. (Right) Median (line) and standard deviation (shaded area) of SWH computed over bins of 10-km. The dynamic collocation method is used to select altimeter data.

of data.

Figure 9 shows the normalized bias and the scatter index between S3A (PLRM, SAR and LR-RMC) and in situ data for each buoy as a function of the distance between the buoy and the nearest coastline. First, we see that most (67%) of the European buoys are located within 50 km from the coast, while the furthest offshore buoys (namely A121 and A122 amidst the North Sea) are moored as far as 240km from the coast. The circle's colors indicate the mean SWH for each buoy, which varies between 0.8m and 3.6m. The

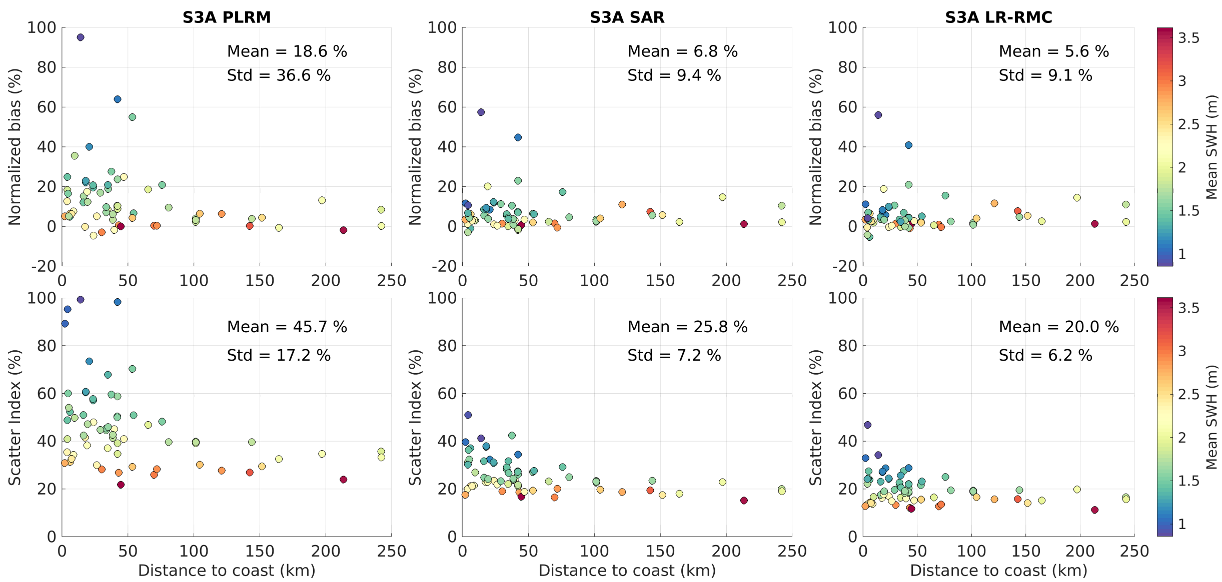

Figure 9: Nbias (upper panels) and SI (lower panels) computed from the differences between S3A PLRM (left panels), SAR (middle panels) and LR-RMC (right panels) and buoy SWH data at each buoy as a function of the distance of the buoy to the coast. The data pairing is based on the dynamic collocation method. Colorscale indicates the mean SWH at the location of each buoy.

first pattern common to all S3A products is the increased error towards the coast. More specifically, the range of the normalized bias increases from [-2 ;

20]% in the 50-250km coastal strip to [-5 ; 95]% in the 2-50km coastal strip. Likewise, the range of SI increases from [11 ; 25]% in the 50-250km coastal strip to [10 ; 100]% in the 2-50km coastal strip. Moreover, the systematic error is positive for a large majority of the buoys, indicating an overestimate of S3A SWH data wrt. buoy data, which is particularly pronounced near the coast, particularly with the S3A PLRM processing. If we now compare the different products, we can see the clear improvement of SAR and LR-RMC data compared to the PLRM data. The mean normalized bias decreases from 18.6% (PLRM) to 5.6% (LR-RMC) and the mean SI decreases from 45.7% (PLRM) to 20% (LR-RMC). On average, the LR-RMC processing presents the best performance, with a reduction of the error of approximately 20% with respect to SAR data. This improved performance of LR-RMC with respect to SAR processing can be attributed to the larger effective footprint averaging out the effects of long ocean waves (swells) that are known to impact SAR-mode measurements (Rieu et al., 2021) as well as the smaller incoherent integration time limiting surface movement effects (Moreau et al., 2021). The fact that S3A performance starts decreasing from 50km-onwards despite lower effective footprint areas could be the result of two factors: first, the buoy distance to the coast does not necessarily reflect the actual position of the paired altimeter records, which may occur closer to the coast; then, the average SWH records decrease towards the coast, which result in higher fraction of low SWH that are measured with limited accuracy by radar altimeters (see Figure 8). In order to investigate these impacts, the error metrics were binned as a function of the altimeter distance to the coast (Figure 10). We see that the errors increase towards the coast, and that

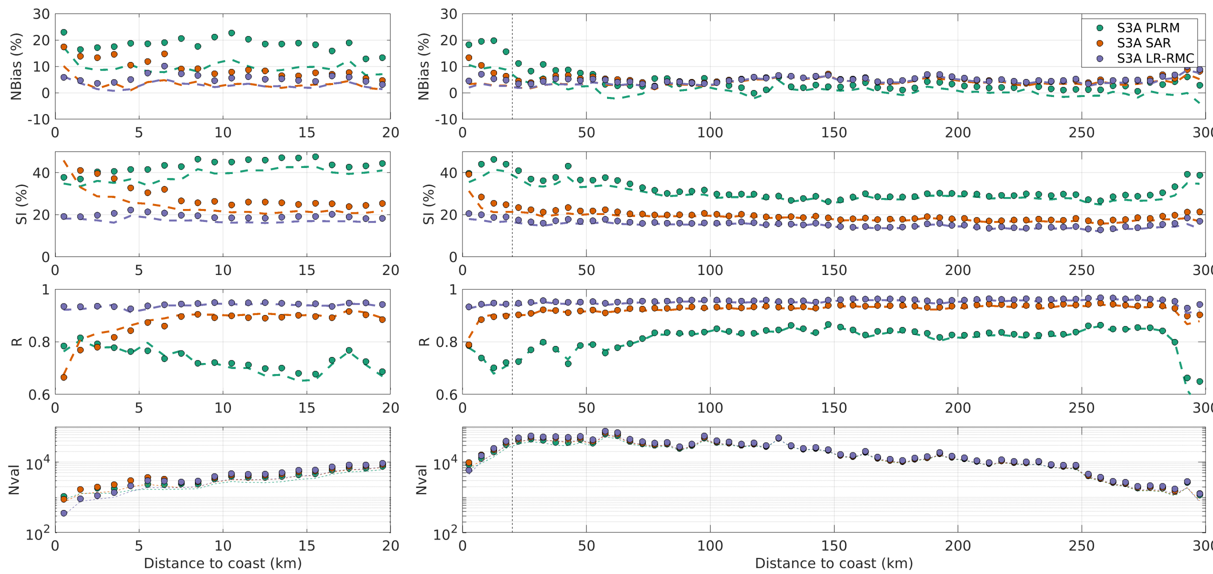

Figure 10: Nbias (top-row panels), SI (second-row panels), R (third-row panels) and number of valid values NVal (bottom-row panels) computed from the differences between S3A PLRM (blue circles), SAR (red circles) and LR-RMC (green circles) and model SWH data as a function of the distance of the altimeter record to the coast, with bins of 10-km width. Left panels correspond to a zoom over the 0-20km from the coast, using bins of 1-km width.

the normalized bias is mostly positive (around 5%) for all products. Yet, in comparison to the previous analysis using the buoy positions instead of the altimeter positions (Figure 9), the bias increase occurs closer to the coast, at around 40km for PLRM and 20 km for SAR data. For LR-RMC the bias remains very stable (between 0-10%) up to 1km from the coast (see zoom over the 0-20km coastal strip on the left panels). For SI, we see that the error starts increasing at around 70km for PLRM data. For SAR data SI presents a sharp increases at around 7km from the coast. And here again, LR-RMC data remains very stable (between 10-22%) up to 1km from the coast. Finally, the correlation coefficient R confirm the previous tendencies, with decreasing values at around 70km for PLRM data, a sharp decrease at around 10km for SAR data, and a much more stable trend (above 0.9) for LR-RMC data. If we compare the three products, we see that the biases are very similar (slightly lower for PLRM) in the 50-300km region, while they become much lower for SAR and LR-RMC data in the 0-50km region. For SI and R, there is a significant offset between PLRM error level on one side, and SAR and LR-RMC error level on the other side. Also, the systematically lower SI and R values obtained with LR-RMC compared to SAR can be explained by the better spatial average of the surface elevation resulting from the larger effective footprint and mitigating the swell impact, and the lowest incoherent integration time (0.05 s compared to 2.5 s for the unfocused SAR data processing), limiting possible surface movement effects. The shoreward increase in the SI and R offset between SAR and LR-RMC could be the signature of the impact long ocean wave effects on SAR measurements, as wave frequency and directional spreads both reduce near the coast due to coastal sheltering, depth induced refraction and fetch reduction. Overall, the LR-RMC data give the best scores in both offshore and nearshore waters, confirming the excellent performance of the LR-RMC processing method. In the 0-20km region, the average scores for LR-RMC are : NBias = 2.9%, SI = 17.2% and R = 0.94. The number of valid values was also binned as a function of the distance to the coast. While these numbers are fairly similar between products up to 7km from the coast, we can see that it drops more rapidly for LR-RMC in the 1-7km region. This reflects the different data editing information provided for each product which are more or less stringent in the coastal zone. With the LR-RMC product, this information seems to be particularly efficient to reject invalid altimeter record in the coastal zone, as also evidenced by Schlembach et al. (2020), which likely contributes to the improved performance compared to the SAR data.

To estimate the contribution of inaccurate low sea state measurements on this coastal performance analysis, we computed the same metrics after excluding all buoy measurements below 1 m. The results are represented as dashed lines on Figure 10. Overall, we note a systematic reduction of Nbias and SI, which is more pronounced in the 0-20km coastal strip. This effect is particularly visible on PLRM and SAR measurements within 0-5km from the coast, with NBias reducing from 18% to 10% and from 13% to 3%, and SI reducing from 40% to 36% and from 39% to 31%, for PLRM and SAR respectively. Finally, the impact of the different data pairing methods on the S3A coastal performance analysis is investigated. The Nbias and SI are computed considering all altimeter measurements within 0-10km, 10-20km and 20-50km from the coast obtained with the different data pairing methods

(Table 2). Overall we note a large spread of the metrics when different data pairing methods are used, which confirms the strong impact of the sampling on the results. These spreads are particularly pronounced in the 0-10km region, and less pronounced in the 20-50km region. We see that the best scores are systematically obtained with the polygon or dynamic collocation methods, while the dynamic correction method presents significant improvements with respect to static method, mostly in the 20-50km region. In the 0-10km region, this model-based method can even reduce the performance, possibly because of inaccurate model results in the near coastal zone. Comparing the different S3A processing modes, the LR-RMC clearly outperforms the PLRM and SAR data, possibly due to its larger effective footprint (inducing dependencies between consecutive measurements) and smaller incoherent integration time, as well as its improved flagging of outliers.

Method	PLRM		SAR		LR-RMC	
	Nbias (%)	SI (%)	Nbias (%)	SI (%)	Nbias (%)	SI (%)
			0-10km			
Static 50km	18.2	49.8	1.7	49.1	-3.0	29.9
Polygon	13.0	37.8	9.2	26.2	8.5	17.6
Dynamic collocation	19.0	42.2	11.7	33.7	6.3	20.3
Dynamic correction	53.7	63.0	26.0	51.7	10.0	24.3
			10-20km			
Static 50km	24.8	48.9	7.0	31.5	4.0	25.3
Polygon	14.8	44.3	8.9	24.9	6.9	18.8
Dynamic collocation	17.2	45.0	6.9	25.2	5.1	19.0
Dynamic correction	27.9	49.9	9.2	27.7	6.0	19.9
			20-50km			
Static 50km	17.7	43.6	9.8	26.7	8.2	21.7
Polygon	9.3	37.5	4.0	22.3	2.7	16.5
Dynamic collocation	9.2	38.6	5.4	22.5	4.5	17.1
Dynamic correction	13.6	42.5	6.0	23.6	4.5	18.0

Table 2: Nbias and SI between buoy and S3A SWH measurements (PLRM, SAR and LR-RMC), for the following coastal regions: 0-10km, 10-20km and 20-50km from the coast.

5. Conclusion

Sea state variability is strongly enhanced in the coastal zone due to interactions between waves, currents, winds, bathymetry and coastline geometry. In Section 4.1, we have used a high-resolution wave hindcast in order to estimate the spatial scales over which the SWH measured by European coastal buoys can be considered homogeneous (in a statistical sense). Our results show that these so-called buoy representativeness areas (here defined as the region where the modeled spatial representativeness systematic and random errors are below 5%) vary strongly in size and shape, depending on the buoy environmental settings, and can be as small as an equivalent disk's radius of 1.5km (see Figure 2). Knowing that the conventional data pairing (or collocation) methods used to compare altimeter and in situ data in deep water usually assumes sea state homogeneity over 50 to 100 km, it is clear that such methods cannot be directly applied for the validation of coastal altimeter SWH data without impairing the results. To demonstrate it, we computed in Section 3.2 statistical error metrics over samples obtained with several data pairing methods, accounting or not for sea state variability, for comparing S3A and in situ SWH in the coastal zone. Our results confirm the efficiency of model-based data pairing methods to reduce spatial representativeness errors related to coastal sea state variability, while preserving a sufficiently large sample from the population. For instance, in comparison to the 50-km static collocation method, the dynamic collocation method gives a 30% lower Nbias and a 22% lower SI for a 22% larger sampling size (see Figure 5).We also investigated the impact of the data pairing methods on the geographical sampling and SWH distribution of coastal measurements and we showed that the seaward asymmetry of the coastal sampling could partially explain systematic errors observed between S3A and buoy measurements, and that the increased fraction of low values (below 1m) in the SWH distribution could induce a significant increase of the altimeter measurement uncertainties in the coastal zone. While this impact could be highly significant in coastal altimetry validation results, it has been little documented so far. Having gained a better understanding of the role of data pairing methods on coastal altimetry validation, we evaluated its impact on the coastal performance of S3A SWH measurements obtained with the PLRM, SAR and LR-RMC processing methods (Section 4.4). Our results show that all three products present increased error levels in the 0-50km region . This can be explained by model limitations to reproduce the real world sea state variability and by the lower sea state conditions that characterized sheltered near-coastal region and that are inaccurately measured by Ku-band altimeter sensors. Ignoring these low sea state measurements significantly reduces the range of error levels in the 0-50km region, particularly for the SAR and LR-RMC data (see Figure 9). . These comparisons clearly show the improved performance of SAR and LR-RMC products compared to PLRM, in both offshore and coastal waters (see Figure 10). They also reveal the consistency of the S3A LR-RMC measurements up to 1km from the coast partially due to the filtering effect inherent to LR-RMC processing and by an efficient data editing procedure, which results in stable error metrics over the 0-20km region, with average NBias = 2.4%, SI = 18.9% and R = 0.95. However, these findings were shown to be highly dependent on the selected data pairing method and the buoy dataset, which claims for deeper analysis in future coastal validation studies. Given the development of dedicated SAR altimetry coastal processors, such as the COastal Retracker for SAR ALtimetry (CORAL V1, Schlembach et al., 2022) or the one developed within the SAR Radar Altimetry for Coastal Zone and Inland Water Level project (HYDROCOASTAL, https://www.satoc.eu/projects/hydrocoastal/index.html), it seems particularly relevant to apply optimized data pairing methods in order to assess the performance of these processors in the coastal zone.

6. Acknowledgments

This research is funded by the European Space Agency through the Sea State CCI project of the Climate Change Initiative (CCI) (ESA ESRIN, Contract 4000123651/18/I-NB).

References

Abdalla, S., Cavaleri, L., 2002. Effect of wind variability and variable air density on wave modeling. Journal of Geophysical Research: Oceans 107, 17–1–17–17. URL: https://onlinelibrary.wiley.com/doi/abs/10.1029/2000JC000639, doi:10.1029/2000JC000639. _eprint: https://onlinelibrary.wiley.com/doi/pdf/10.1029/2000JC000

Accensi, M., Alday Gonzalez, M.F., Maisondieu, C., Raillard, N., Darbynian, D., Old, C., Sellar, B., Thilleul, O., Perignon, Y., Payne, G., O'Boyle, L., Fernandez, L., Dias, F., Chumbinho, R., Guitton, G., 2021. ResourceCODE framework: A high-resolution wave parameter dataset for the European Shelf and analysis toolbox, in: EWTEC 2021, Plymouth, UK. URL: https://archimer.ifremer.fr/doc/00736/84812/.

Alday, M., Accensi, M., Ardhuin, F., Dodet, G., 2021. A global wave parameter database for geophysical applications. Part 3: Improved forcing and spectral resolution. Ocean Modelling 166, 101848. URL: https://www.sciencedirect.com/science/article/pii/S1463500321001001, doi:10.1016/j.ocemod.2021.101848.

Alday, M., Ardhuin, F., Dodet, G., Accensi, M., 2022. Accuracy of numerical wave model results: Application to the Atlantic coasts of Europe. EGUsphere , 1–39URL: https://egusphere.copernicus.org/preprints/2022/egusphere-2022-481/, doi:10.5194/egusphere-2022-481. publisher: Copernicus GmbH.

Ardhuin, F., Roland, A., Dumas, F., Bennis, A.C., Sentchev, A., Forget, P., Wolf, J., Girard, F., Osuna, P., Benoit, M., 2012. Numerical Wave Modeling in Conditions with Strong Currents: Dissipation, Refraction, and Relative Wind. Journal of Physical Oceanography 42, 2101–2120. URL: http://journals.ametsoc.org/doi/abs/10.1175/JPO-D-11-0220.1, doi:10.1175/JPO-D-11-0220.1.

Ardhuin, F., Stopa, J.E., Chapron, B., Collard, F., Husson, R., Jensen, R.E., Johannessen, J., Mouche, A., Passaro, M., Quartly, G.D., Swail, V., Young, I., 2019. Observing Sea States. Frontiers in Marine Science 6. URL: https://www.frontiersin.org/articles/10.3389/fmars.2019.00124/full, doi:10.3389/fmars.2019.00124.

Birol, F., Fuller, N., Lyard, F., Cancet, M., Niño, F., Delebecque, C., Fleury, S., Toublanc, F., Melet, A., Saraceno, M., Léger, F., 2017. Coastal applications from nadir altimetry: Example of the X-TRACK regional products. Advances in Space Research 59, 936 – 953. URL: http://www.sciencedirect.com/science/article/pii/S0273117716306317, doi:https://doi.org/10.1016/j.asr.2016.11.005.

Boy, F., Desjonqueres, J.D., Picot, N., Moreau, T., Raynal, M., 2017. CryoSat-2 SAR-Mode over Oceans: Processing Methods, Global Assessment, and Benefits. IEEE Transactions on Geoscience and Remote Sensing 55, 148–158. doi:10.1109/TGRS.2016.2601958.

Chelton, D.B., Walsh, E.J., MacArthur, J.L., 1989. Pulse Compression and Sea Level Tracking in Satellite Altimetry. Journal of Atmospheric and Oceanic Technology 6, 407–438. doi:10.1175/1520-0426(1989)006¡0407:PCASLT¿2.0.CO;2.

Dodet, G., Bertin, X., Bouchette, F., Gravelle, M., Testut, L., Wöppelmann, G., 2019. Characterization of Sea-level Variations Along the Metropolitan Coasts of France: Waves, Tides, Storm Surges and Long-term Changes. Journal of Coastal Research 88, 10–24. URL: https://bioone.org/journals/Journal-of-Coastal-Research/volume-88/issue-sp1/SI88 doi:10.2112/SI88-003.1.

Fanti, V., Ferreira, , Kümmerer, V., Loureiro, C., 2023. Improved estimates of extreme wave conditions in coastal areas from calibrated global reanalyses. Communications Earth & Environment 4, 1–11. URL: https://www.nature.com/articles/s43247-023-00819-0, doi:10.1038/s43247-023-00819-0. number: 1 Publisher: Nature Publishing Group.

Fernandes, M.J., Lázaro, C., Ablain, M., Pires, N., 2015. Improved wet path delays for all ESA and reference altimetric missions. Remote Sensing of Environment 169, 50–74. URL: https://www.sciencedirect.com/science/article/pii/S003442571530081X, doi:10.1016/j.rse.2015.07.023.

Hersbach, H., Bell, B., Berrisford, P., Hirahara, S., Horányi, A., Muñoz-Sabater, J., Nicolas, J., Peubey, C., Radu, R., Schepers, D., Simmons, A., Soci, C., Abdalla, S., Abellan, X., Balsamo, G., Bechtold, P., Biavati, G., Bidlot, J., Bonavita, M., Chiara, G.D., Dahlgren, P., Dee, D., Diamantakis, M., Dragani, R., Flemming, J., Forbes, R., Fuentes, M., Geer, A., Haimberger, L., Healy, S., Hogan, R.J., Hólm, E., Janisková, M., Keeley, S., Laloyaux, P., Lopez, P., Lupu, C., Radnoti, G., Rosnay, P.d., Rozum, I., Vamborg, F., Villaume, S., Thépaut, J.N., 2020. The ERA5 global reanalysis. Quarterly Journal of the Royal Meteorological Society 146, 1999–2049. URL: https://rmets.onlinelibrary.wiley.com/doi/abs/10.1002/qj.3803, doi:10.1002/qj.3803. _eprint: https://rmets.onlinelibrary.wiley.com/doi/pdf/10.1002/qj.3803.

Hithin, N.K., Remya, P.G., Balakrishnan Nair, T.M., Harikumar, R., Kumar, R., Nayak, S., 2015. Validation and Intercomparison of SARAL/AltiKa and PISTACH-Derived Coastal Wave Heights Using In-Situ Measurements. IEEE Journal of Selected Topics in Applied Earth Observations and Remote Sensing 8, 4120–4129. doi:10.1109/JSTARS.2015.2418251. conference Name: IEEE Journal of Selected Topics in Applied Earth Observations and Remote Sensing.

Jackson, F.C., 1979. The reflection of impulses from a nonlinear random sea. Journal of Geophysical Research: Oceans 84, 4939–4943. URL: https://onlinelibrary.wiley.com/doi/abs/10.1029/JC084iC08p04939, doi:10.1029/JC084iC08p04939.

Janssen, P.A.E.M., Abdalla, S., Hersbach, H., Bidlot, J.R., 2007. Error Estimation of Buoy, Satellite, and Model Wave Height Data. Journal of Atmospheric and Oceanic Technology 24, 1665–1677. URL: https://journals.ametsoc.org/jtech/article/24/9/1665/2940/Error-Estimation-of-Bu
doi:10.1175/JTECH2069.1. publisher: American Meteorological Society.

Jiang, H., 2020. Indirect Validation of Ocean Remote Sensing Data via Numerical Model: An Example of Wave Heights from Altimeter. Remote Sensing 12, 2627. URL: https://www.mdpi.com/2072-4292/12/16/2627, doi:10.3390/rs12162627. number: 16 Publisher: Multidisciplinary Digital Publishing Institute.

Jiang, H., Fu, G., Ren, L., 2022. Evaluation of Coastal Altimeter Wave Height Observations Using Dynamic Collocation. IEEE Transactions on Geoscience and Remote Sensing 60, 1–8. doi:10.1109/TGRS.2022.3198430. conference Name: IEEE Transactions on Geoscience and Remote Sensing.

Moreau, T., Cadier, E., Boy, F., Aublanc, J., Rieu, P., Raynal, M., Labroue, S., Thibaut, P., Dibarboure, G., Picot, N., Phalippou, L., Demeestere, F., Borde, F., Mavrocordatos, C., 2021. High-performance altimeter Doppler processing for measuring sea level height under varying sea state conditions. Advances in Space Research 67, 1870–1886. URL: https://www.sciencedirect.com/science/article/pii/S027311772030911X, doi:10.1016/j.asr.2020.12.038.

Moreau, T., Tran, N., Aublanc, J., Tison, C., Le Gac, S., Boy, F., 2018. Impact of long ocean waves on wave height retrieval from SAR altimetry data. Advances in Space Research 62, 1434–1444. URL: https://www.sciencedirect.com/science/article/pii/S0273117718304708, doi:10.1016/j.asr.2018.06.004.

Mureau, G., Dodet, G., Suanez, S., 2022. Characterizing sea state variability along the French Atlantic coast. Proceedings of the XVIIèmes Journées Nationales Génie Côtier – Génie Civil , 129–142doi:10.5150/jngcgc.2022.015.

Nencioli, F., Quartly, G.D., 2019. Evaluation of Sentinel-3A Wave Height Observations Near the Coast of Southwest England. Remote Sensing 11, 2998. URL: https://www.mdpi.com/2072-4292/11/24/2998, doi:10.3390/rs11242998. number: 24 Publisher: Multidisciplinary Digital Publishing Institute.

Passaro, M., Hemer, M.A., Quartly, G.D., Schwatke, C., Dettmering, D., Seitz, F., 2021. Global coastal attenuation of wind-waves observed with radar altimetry. Nature Communications 12, 3812. URL: https://www.nature.com/articles/s41467-021-23982-4, doi:10.1038/s41467-021-23982-4.

Passaro, M., Rose, S.K., Andersen, O.B., Boergens, E., Calafat, F.M., Dettmering, D., Benveniste, J., 2018. ALES+: Adapting a homogenous ocean retracker for satellite altimetry to sea ice leads, coastal and inland waters. Remote Sensing of Environment 211, 456–471. URL: http://www.sciencedirect.com/science/article/pii/S0034425718300920, doi:10.1016/j.rse.2018.02.074.

Raney, R., 1998. The delay/Doppler radar altimeter. IEEE Transactions on Geoscience and Remote Sensing 36, 1578–1588. doi:10.1109/36.718861. conference Name: IEEE Transactions on Geoscience and Remote Sensing.

Schlembach, F., Passaro, M., Dettmering, D., Bidlot, J., Seitz, F., 2022. Interference-sensitive coastal SAR altimetry retracking strategy for measuring significant wave height. Remote Sensing of Environment 274, 112968. URL: https://www.sciencedirect.com/science/article/pii/S0034425722000827, doi:10.1016/j.rse.2022.112968.

Schlembach, F., Passaro, M., Quartly, G.D., Kurekin, A., Nencioli, F., Dodet, G., Piollé, J.F., Ardhuin, F., Bidlot, J., Schwatke, C., Seitz, F., Cipollini, P., Donlon, C., 2020. Round Robin Assessment of Radar Altimeter Low Resolution Mode and Delay-Doppler Retracking Algorithms for Significant Wave Height. Remote Sensing 12, 1254. URL: https://www.mdpi.com/2072-4292/12/8/1254, doi:10.3390/rs12081254. number: 8 Publisher: Multidisciplinary Digital Publishing Institute.

Smith, W.H.F., Scharroo, R., 2015. Waveform Aliasing in Satellite Radar Altimetry. IEEE Transactions on Geoscience and Remote Sensing 53, 1671–1682. doi:10.1109/TGRS.2014.2331193. conference Name: IEEE Transactions on Geoscience and Remote Sensing.

Tourain, C., Piras, F., Ollivier, A., Hauser, D., Poisson, J.C., Boy, F., Thibaut, P., Hermozo, L., Tison, C., 2021. Benefits of the Adaptive Algorithm for Retracking Altimeter Nadir Echoes: Results From Simulations and CFOSAT/SWIM Observations. IEEE Transactions on Geoscience and Remote Sensing , 1–14doi:10.1109/TGRS.2021.3064236. conference Name: IEEE Transactions on Geoscience and Remote Sensing.

Vignudelli, S., Birol, F., Benveniste, J., Fu, L.L., Picot, N., Raynal, M., Roinard, H., 2019. Satellite Altimetry Measurements of Sea Level in the Coastal Zone. Surveys in Geophysics 40, 1319–1349. URL: https://doi.org/10.1007/s10712-019-09569-1, doi:10.1007/s10712-019-09569-1.

Yaplee, B.S., Shapiro, A., Hammond, D.L., Au, B.D., Uliana, E.A., 1971. Nanosecond Radar Observations of the Ocean Surface from a Stable

Platform. IEEE Transactions on Geoscience Electronics 9, 170–174. doi:10.1109/TGE.1971.271490. conference Name: IEEE Transactions on Geoscience Electronics.